Int. J. Heat Mass Transfer. Vol. 33, No. 2, pp. 229–242, 1990
Printed in Great Britain

0017–9310/90 53.00+0.00
Pergamon Press plc

Phenomenological modelling of non-equilibrium flows with phase change†

G. F. HEWITT and A. H. GOVAN
Thermal Hydraulics Division, B392, Harwell Laboratory, Oxfordshire OX11 0RA, U.K.

(*Received* 20 *March* 1989 *and in final form* 10 *May* 1989)

Abstract—Calculations are described in which new models for deposition and entrainment in annular flow are applied to a variety of conditions in annular and related flows. These include steady adiabatic flow, flow with evaporation, flow with dryout and post-dryout regions, flow with condensation and transient flows. The transient cases considered include both excursions with a flow decrease (transient dryout) and excursions with a flow increase (transient rewetting). Wherever possible, the predictions are compared with experimental data; this shows that the new models give improved predictions in every case. Although it is not possible to make comparisons with experimental data in the case of flow transients leading to rewetting, several new aspects of this process emerged from the calculations. Specifically, it is found that the rewetting rate could be governed either by the progress of a front at which the film flow rate is zero (the reverse of a transient dryout situation) or by a front the velocity of which is limited by the sputtering phenomenon.

1. INTRODUCTION

MANY OF the more interesting phenomena in heat transfer in two-phase single-component flows occur in the annular regime which exists in such flows for qualities above, typically, a few per cent. In such flows, the liquid phase flows partly in a liquid film on the channel wall and partly as entrained droplets in the vapour core. In adiabatic flow, an equilibrium situation may ultimately be reached in which the rate of droplet entrainment is equal and opposite to the rate of droplet deposition. However, in most practical situations, and especially in flows with evaporation or condensation (diabatic flows), there are significant departures from equilibrium. This was first demonstrated experimentally in the 1960s [1–3] and analytical models were subsequently developed [5] which took account of these non-equilibrium effects. These models were subsequently refined and extended to include thermal in addition to hydrodynamic non-equilibrium [6]. The models can be used for complex geometries [7] and also for flow and pressure transients [8]. Although useful results were obtained with the annular flow models, a severe limitation on them has always been the inadequacy of the earlier correlations of entrainment rate and deposition rate of droplets. Over the past few years, an extensive exercise has been carried out to attempt to improve these correlations and to cover a wider range of data. New correlations for entrainment and deposition are described in ref. [9] and this present paper explores the application of these models to some previously-studied problems (steady-state dryout, post-dryout modelling and transient dryout) together with some new applications, namely steady-state saturated condensation and transient rewetting.

2. NEW ANNULAR FLOW MODEL

In the earlier Harwell annular flow modelling code (HANA), somewhat simplified correlations were used for deposition and entrainment. Deposition rate D (kg m^{-2} s^{-1}) was calculated from

$$D = kC \tag{1}$$

where C is the concentration (kg m^{-3}) in the vapour core, calculated on the basis of a homogeneous mixture and k (m s^{-1}) the deposition mass transfer coefficient which, in the earlier models was simply correlated as a function of surface tension. The entrainment rate E (kg m^{-2} s^{-1}) was calculated from the relationship

$$E = kC_E \tag{2}$$

where C_E is the droplet concentration corresponding to the local value of the group $\tau_i\delta/\sigma$ where τ_i is the interfacial shear stress, δ the local film thickness and σ the surface tension. The relationship between C_E and $\tau_i\delta/\sigma$ was determined on the basis of equilibrium flows and it was assumed that the same relationship applied in non-equilibrium flows. There had been several attempts to improve these original correlations (see for instance ref. [7]) and it was also suspected that the deposition rate would not be proportional to the concentration of droplets as suggested by equation (1). Recognition of the droplet concentration effect, and also the fact that a limiting film flow rate occurred below which no entrainment took place, has led to improved correlations which cover a wide range of fluids, system pressures and velocities. Though it is not claimed that these correlations are the ultimate ones in this area, they certainly give a much more realistic prediction of a variety of parameters in annu-

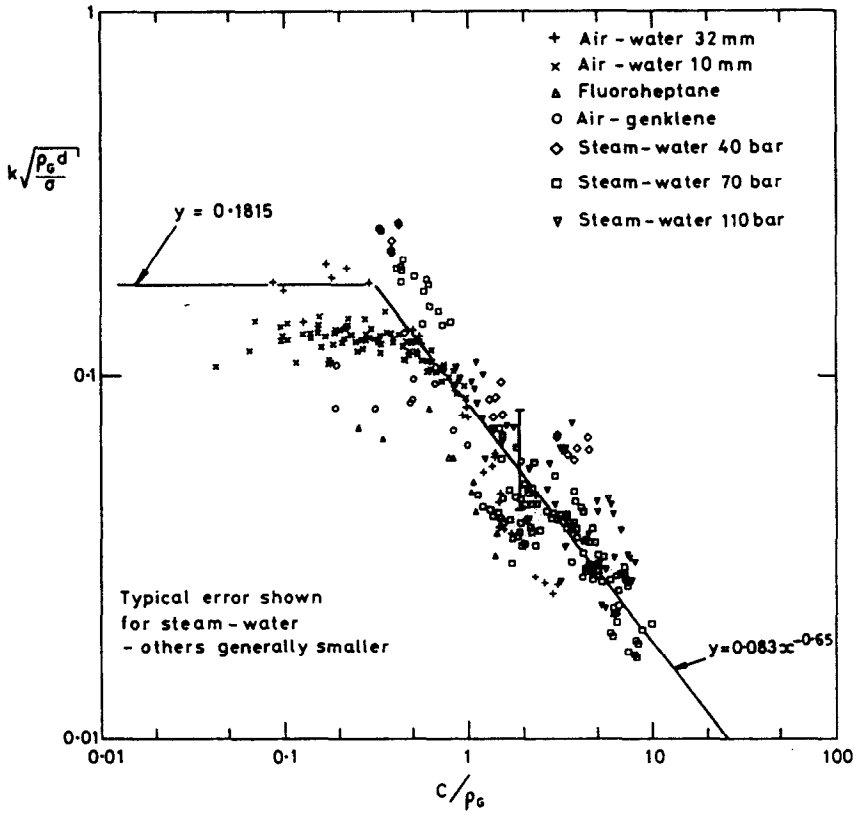

FIG. 1. Deposition correlation.

lar flow. The new correlations are described in ref. [9] and are as follows:

$$k\sqrt{\left(\frac{\rho_G d}{\sigma}\right)} = 0.18 \quad \text{if } C/\rho_G < 0.3 \tag{3}$$

$$k\sqrt{\left(\frac{\rho_G d}{\sigma}\right)} = 0.083(C/\rho_G)^{-0.65} \quad \text{if } C/\rho_G > 0.3 \tag{4}$$

$$E/\dot{m}_G = 5.75\times 10^{-5}\left[(\dot{m}_{LF}-\dot{m}_{LFC})^2\frac{d\rho_L}{\sigma\rho_G^2}\right]^{0.316}$$

$$\text{for } \dot{m}_{LF} > \dot{m}_{LFC} \tag{5}$$

where ρ_G is the gas phase density, d the channel diameter, $\dot{m}_G$ the gas mass flux, $\dot{m}_{LF}$ the flow rate in the liquid film (referred to the total cross-section of the channel), $\dot{m}_{LFC}$ the critical film flow rate for the onset of entrainment and ρ_L the density of the liquid phase. $\dot{m}_{LFC}$ is given by the following relationship [10]:

$$\frac{\dot{m}_{LFC}d}{\eta_L} = Re_{LFC} = \exp\left(5.8504+0.4249\frac{\eta_G}{\eta_L}\sqrt{\left(\frac{\rho_L}{\rho_G}\right)}\right) \tag{6}$$

where η_L and η_G are the viscosities of the liquid and gas phases, respectively. The new correlations are illustrated in Figs. 1 and 2, respectively.

The entrainment and deposition correlations can be used to calculate local film flow rate in annular flow systems by integrating the following expression:

$$\frac{d\dot{m}_{LF}}{dz} = \frac{4}{d}(D-E-\dot{q}/h_{LG}) \tag{7}$$

where the final term represents the change of film flow rate due to phase change, $\dot{q}$ being the heat flux through the wall of the channel and h_{LG} the latent heat of vaporization. Note that $\dot{q}$ is negative for condensation. A major difficulty with equation (7) is that of choosing appropriate boundary conditions. Commonly, the boundary conditions are either known (for instance zero film flow rate at the entrance of the channel in the condensation of the pure vapour) or are arbitrarily estimated (for instance assuming that a given fraction of the liquid phase is in the liquid film at a given quality). The earlier modelling work showed that, for long enough channels, the predictions were relatively insensitive to the assumptions about entrance conditions. A typical assumption was that the boundary condition was for 99% of the fluid to be entrained as droplets at a quality of 0.01. A variety of other boundary assumptions have been and are discussed, for instance, ref. [9]. Broadly speaking, as the models for entrainment and deposition become more sophisticated, the more significant are the boundary conditions and the calculation methods are

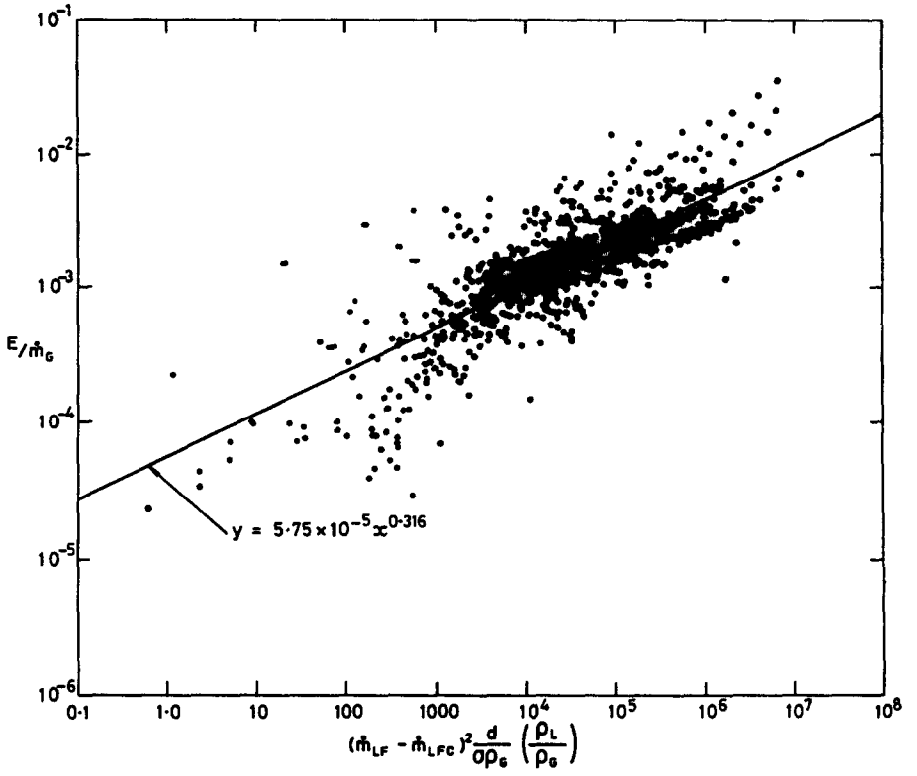

FIG. 2. Entrainment correlation.

significantly affected by the assumed boundary conditions for short tubes and high mass fluxes.

An obvious application of the method is to calculate those conditions under which the film flow rate reaches zero, namely dryout (otherwise known as 'burnout', 'DNB', 'boiling crisis', etc.). However, the method is also useful in estimating local pressure gradients and void fraction (which follows from a knowledge of the film thickness) and as a basis for calculating heat transfer coefficients in both evaporation and condensation. If the liquid film flow rate is known, then the interfacial shear stress and film thickness can be calculated by iterative solution of the 'triangular relationship' between liquid film thickness, interfacial shear stress and liquid film flow rate [11] and a relationship between interfacial shear stress, gas core velocity and liquid film thickness, often referred to as the 'interfacial roughness relationship'. For the latter, we have chosen the simple form given by Wallis [12] which is as follows:

$$f_i = f_{GC}\left[1+360\frac{\delta}{d}\right] \tag{8}$$

where f_{GC} is a single-phase friction factor calculated from the Blasius equation

$$f_{GC} = 0.079(Re_{GC})^{-0.25} \tag{9}$$

where Re_{GC} is the gas core Reynolds number defined as

$$Re_{GC} = (\dot{m}_G + \dot{m}_{LE})\frac{d}{\eta_G} \tag{10}$$

where $\dot{m}_G$ and $\dot{m}_{LE}$ are the gas and entrained droplet mass fluxes, respectively. In more recent work, more complex relationships have developed which take account of the influence of the droplets on gas core turbulence [10] and it is the intention to introduce these complex relationships into the codes in the future. However, for the present calculations, the above relationships were considered sufficiently accurate.

3. STEADY-STATE DRYOUT AND POST-DRYOUT MODELLING

The applications of the new entrainment and deposition correlations to the prediction of dryout were discussed in detail in ref. [9]. The results are typified by those shown in Fig. 3 where predictions for $\dot{m}_{LE}$ in equilibrium adiabatic flow and diabatic flow of steam–water mixtures are compared with the data of Bennett *et al.* [25]. As will be seen, the new correlations for entrainment and deposition give improved predictions.

Whalley *et al.* [6] describe a sophisticated annular flow modelling code (PGR2) which is specifically designed to be extended into the post-dryout region. A 'book keeping' exercise is carried out on the droplets generated and transported in the pre-dryout region so

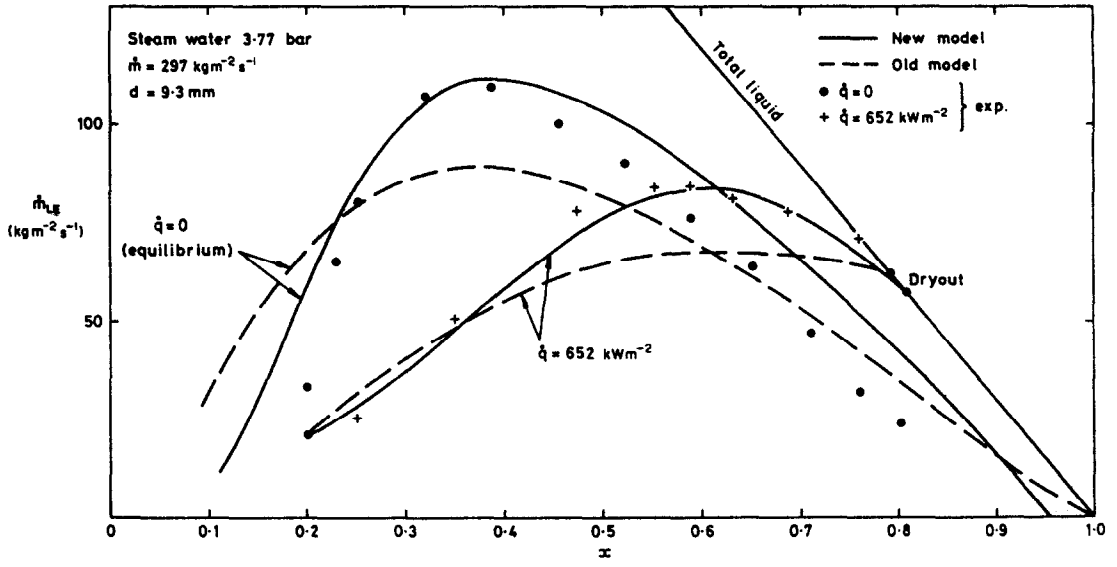

FIG. 3. Comparison with entrainment data of Bennett *et al.* [25].

as to calculate their number density, their size and their velocity at the dryout point. These parameters are important in the subsequent stepwise calculation of the post-dryout behaviour, in which droplet velocities, vapour temperatures and wall temperatures are calculated. The code PGR2 was modified to include the new entrainment and deposition correlations. The new code (PGR3) was applied to the post-dryout data of Bennett *et al.* [4] and some of the results are illustrated in Figs. 4 and 5. Annular flow is assumed to occur at $U_G^* = 1$ where U_G^* is defined as

$$U_G^* = \frac{U_G \rho_G^{1/2}}{\sqrt{(gd(\rho_L - \rho_G))}} \qquad (11)$$

where U_G is the superficial gas velocity and g the acceleration due to gravity. The parameter U_G^* is due to Wallis [13] and a value of $U_G^* = 1$ is considered typical for the onset of annular flow. Two alternative conditions were assumed at the onset of annular flow, serving as boundary conditions for the integration of equation (7), namely that the fraction entrained ε_0 is either 0.01 or 0.99. This initial assumption has little effect at lower mass fluxes (Fig. 4) but causes a significant change in the position of dryout at higher mass fluxes (Fig. 5). As had been found previously, the assumption of a high initial entrainment is more consistent with the experimental data. In both cases, the revised code (PGR3) predicts the post-dryout temperatures reasonably well though there is some dis-

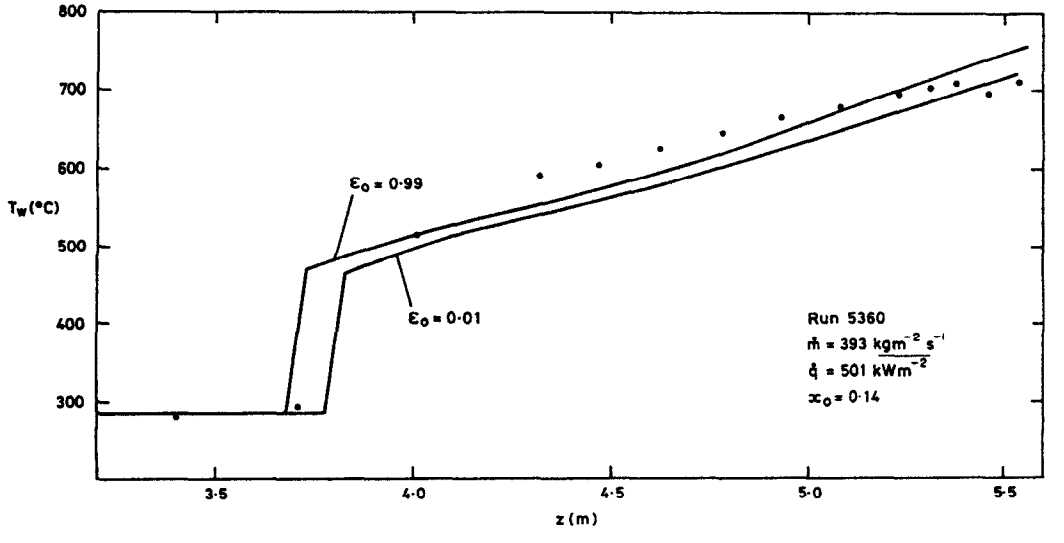

FIG. 4. Comparison with post-dryout data—low mass flux.

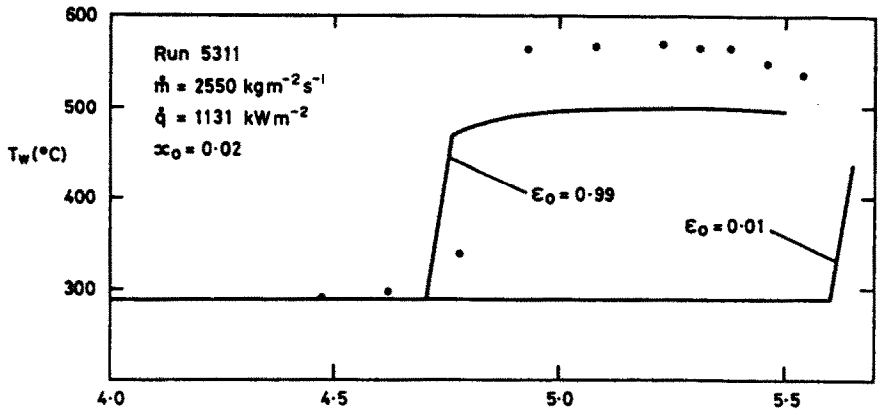

FIG. 5. Comparison with post-dryout data—high mass flux.

crepancy at the higher mass flux, possibly associated with a suppression of the turbulence in the vapour core due to the presence of the droplets.

It should be noted that, in Figs. 4 and 5, the initial temperature rise at dryout corresponds to a change from a film evaporation regime to a regime of heat transfer to the vapour phase. The initial temperature rise is calculated assuming saturated vapour and using a vapour heat transfer coefficient calculated from the Heineman [14] equation. The good performance of this rather simple calculation of initial temperature jump would be found extremely useful in considering rewetting transients as discussed below.

4. STEADY-STATE SATURATED CONDENSATION

Equation (7) can also be applied to the calculation of film mass flux distribution in condensation systems. Here, $\dot{q}$ is negative and the boundary conditions, for an initially saturated vapour, are clearly easier to establish than those in evaporation, corresponding to zero film flow rate at the entrance of the channel. To compare evaporation and condensation, some calculations have been carried out using the new model for precisely the same conditions as was illustrated in Fig. 3 for evaporation. Figures 6 and 8 present the results of this calculation. Figure 6 shows the predicted entrained mass fluxes for the condensation rate for a heat flux which is identical to that for the equivalent case for evaporation (652 kW m^{-2}). Condensation in upwards flow is assumed and, initially, there is no entrainment until the liquid film flow rate reaches the critical value ($\dot{m}_{LFC}$). As the flow proceeds up the channel, with decreasing quality as the vapour condenses, the entrained liquid flow is initially lower than the equilibrium value. However, as the equilibrium value passes through a peak with decreasing quality, then the value for the condensing flow begins to exceed equilibrium as illustrated. It will be seen from Fig. 6 that the entrained flow (and hence the film flow) for equilibrium, for condensation and for evaporation only adventitiously correspond at certain points.

The pressure gradient can be calculated as a function of local quality for the various curves illustrated in Fig. 6. This is carried out by iterative solution of equation (8) and the 'triangular relationship' equation [11, 15]

$$\dot{m}_{LF} = \frac{4\delta}{d}\sqrt{\left(\frac{2\tau_i \rho_L}{f_{LF}}\right)} \tag{12}$$

where f_{LF} is the liquid film friction factor and τ_i the interfacial shear stress estimated from equation (8) by

$$\tau_i = \tfrac{1}{2}\rho_{GC} V_{GC}^2 f_i \tag{13}$$

where ρ_{GC} is the homogeneous gas core density given by

$$\rho_{GC} = \frac{\dot{m}_{LE} + \dot{m}_G}{\dfrac{\dot{m}_{LE}}{\rho_L} + \dfrac{\dot{m}_G}{\rho_G}} \tag{14}$$

and V_{GC} is the homogeneous gas core velocity given by (assuming the thickness of the film is small)

$$V_{GC} = \frac{\dot{m}_G}{\rho_G} + \frac{\dot{m}_{LE}}{\rho_L} = \frac{\dot{m}_G + \dot{m}_{LE}}{\rho_{GC}}. \tag{15}$$

The frictional pressure gradient is then given by

$$\left(\frac{dp}{dz}\right)_F = \frac{4\tau_i}{d}. \tag{16}$$

For the conditions discussed here, the frictional and total pressure gradients are nearly equal since the accelerational and gravitational components are small. The 'thin film' approximation would, of course, be less valid the lower the quality.

At any given quality, the pressure gradient varies with the fraction entrained. For the conditions shown in Fig. 6, the relationship between the frictional pressure gradient and the entrained fraction was determined at several qualities as illustrated in Fig. 7. As can be seen, the frictional pressure gradient generally

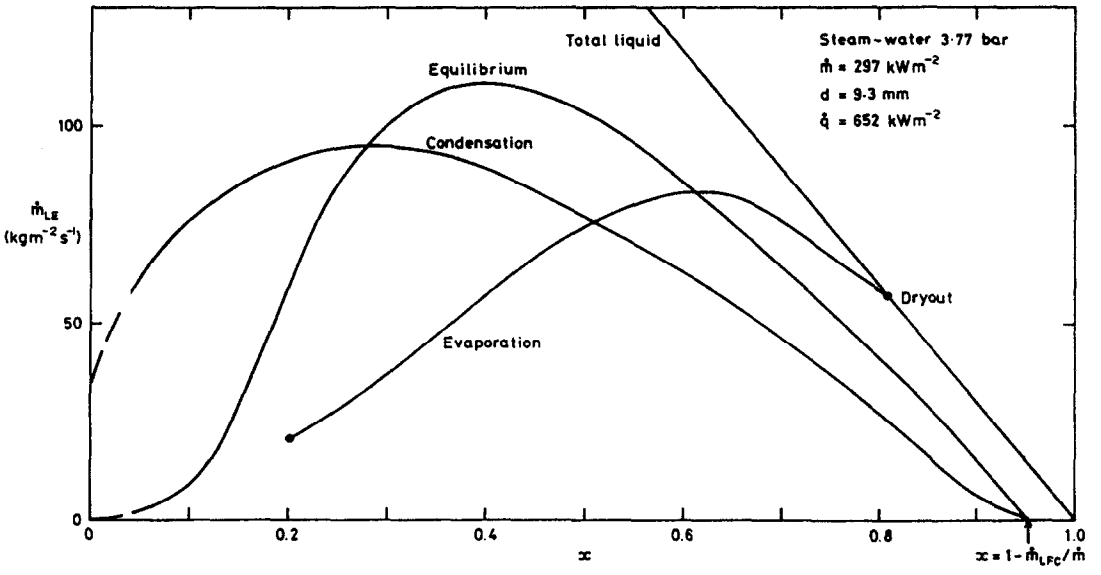

FIG. 6. Entrainment in evaporating and condensing flows.

decreases as the fraction of the liquid which is in the form of entrained droplets increases. At low qualities, however, there is an initial increase reflecting the fact that the increase in ρ_{GC} offsets the decrease in interfacial roughness as the film thickness decreases and the pressure gradient passes through a maximum.

Pressure gradients were determined along the loci shown in Fig. 6 and these values are plotted in Fig. 8. As can be seen, the values for pressure gradient at a given local quality differ between the cases of condensation, evaporation and hydrodynamic equilibrium flows. Over quite a wide range, the pressure gradients for condensation are significantly higher than those for equilibrium and for evaporation. In the latter case, there is a pronounced minimum in the pressure gradient at the dryout point. These differences in pressure gradient (and hence interfacial shear stress) may be crucial in analysis of heat transfer data for condensation and evaporation. It would be expected that there would be significant differences in the heat transfer coefficient reflecting the differences in local entrainment.

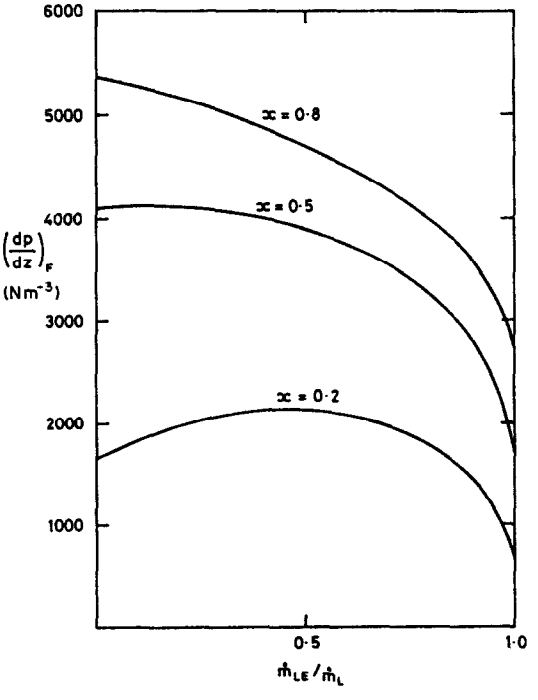

FIG. 7. Variation of pressure gradient with entrained fraction.

5. TRANSIENT DRYOUT

The original Harwell annular flow model has been applied to the calculation of dryout under flow and pressure transients by James and Whalley [8], the work being further extended by Whalley *et al.* [16]. The transient code (PWJ1) gives a numerical solution of the following transient mass and energy balance equations:

$$\frac{\partial}{\partial t}[\rho_L(1-\varepsilon_c)]+\frac{\partial \dot{m}_{LF}}{\partial z}=\frac{4}{d}(D-E-\dot{q}/h_{LG}-F_{LF}) \tag{17}$$

$$\frac{\partial}{\partial t}[\rho_L\varepsilon_c\varepsilon_d]+\frac{\partial \dot{m}_{LE}}{\partial z}=\frac{4}{d}(E-D-F_{LE}) \tag{18}$$

$$\frac{\partial}{\partial t}[\rho_G\varepsilon_c(1-\varepsilon_d)]+\frac{\partial \dot{m}_G}{\partial z}=\frac{4}{d}(\dot{q}/h_{LG}+F_{LF}+F_{LE}) \tag{19}$$

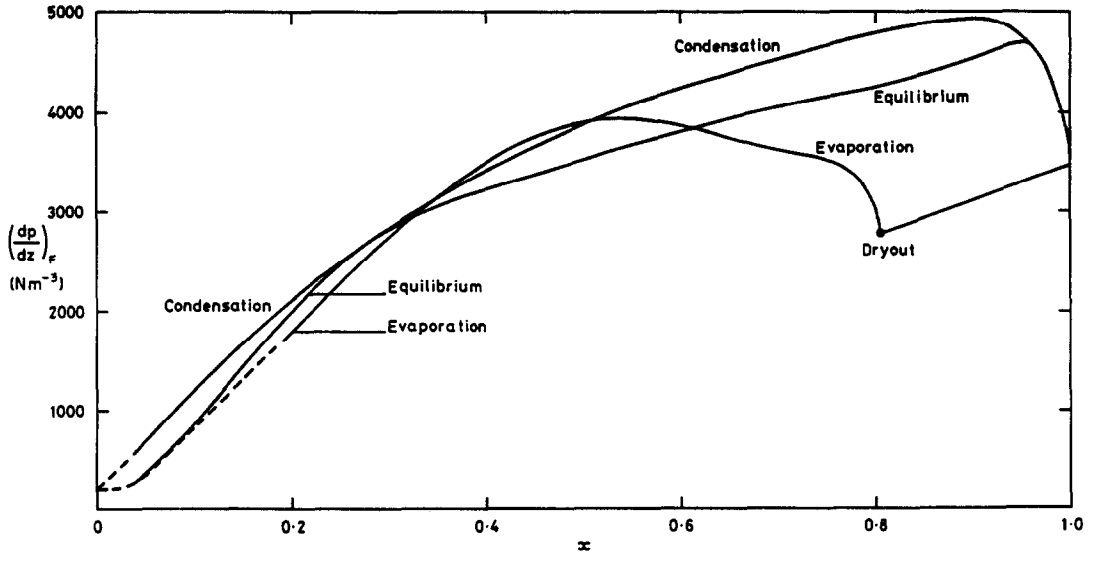

FIG. 8. Pressure gradient in evaporating and condensing flows.

$$\frac{\partial}{\partial t}[\rho_L u_L(1-\varepsilon_c)+\rho_L u_L \varepsilon_c \varepsilon_d+\varepsilon_c(1-\varepsilon_d)\rho_G u_G]$$

$$+\frac{\partial}{\partial z}(h_L \dot{m}_{LF}+h_L \dot{m}_{LE}+h_G \dot{m}_G)=\frac{4\dot{q}}{d} \quad (20)$$

where ε_c is the fraction of the cross-section occupied by the gas core and ε_d is the fraction of the gas core cross-section which is occupied by the entrained droplets. F_{LE} and F_{LF} are the rates of flashing of vapour from the droplets and the liquid film, respectively, each referred to the channel peripheral area. Flashing occurs due to changes in pressure with time and with distance along the channel; in the calculations described in the present paper, these flashing terms are negligible. In equation (20), u_L and u_G are the internal energies and h_L and h_G the enthalpies for the liquid and gas phases, respectively. ε_d is calculated assuming that the flow in the core is homogeneous and ε_c is calculated from the value of film thickness estimated by the methods described above for the steady state. The transient equations are solved in a similar way to the steady-state equations (i.e. using Gear's [17] predictor–corrector method) for the variation with distance with time derivatives being approximated by one-step backward differences.

In the work described here, the code was modified to include the new entrainment and deposition correlations (illustrated in Figs. 1 and 2 and given in equations (3)–(6)). The new code (PWJ1A) was used for most of the calculations described here, but calculations were also carried out with the original code in some cases for comparison.

In order to establish comparisons with the early calculations, the first series of runs was carried out against the high pressure (70 bar) steam–water data of Moxon and Edwards [18]. The results are illustrated in Table 1. In the Moxon and Edwards experiments, the mass flux was decreased with time according to the expression

$$\dot{m}(t) = 786+1926\exp(-t/0.275)\ (\mathrm{kg\,m^{-2}\,s^{-1}}). \quad (21)$$

The results of the comparisons with the Moxon and Edwards experiments are shown in Table 1. In three out of four of the cases considered, the new model gave somewhat closer agreement with the experiment than the earlier model. In steady-state flows, the new correlations for entrainment predict a slower approach to equilibrium along the channel [9] and this is consistent with the longer predicted times to dryout. The model still predicts slightly shorter times to dryout than the experiment but the agreement is, nevertheless, very good. The remaining difference may partly reflect the assumption on initial entrainment. Also shown in Table 1 are values calculated for the pseudo steady state. Here, it is assumed that the total flow rate at the dryout point is equal to that at the entrance of the tube and that storage of the liquid along the tube is negligible. The pseudo steady-state calculations give times to dryout which are grossly below experimental values and the values predicted by the full transient model.

The new model was also used to predict the flow transient experiments of Celata *et al.* [19]. These experiments were carried out using Refrigerant 12 in a 7.72 mm diameter tube, pressures ranging from 1.2 to 2.75 MPa. The mass flow rate at the entrance of the channel was decreased with time in a manner approximated by the following characteristic equation:

Table 1. Comparison with the data of Moxon and Edwards

Run No.	Heat flux (kW m^{-2})	Subcooling (kJ kg^{-1})	Time to dryout (s) Experiment	Old model (PWJ1)	New model (PWJ1A)	New model pseudo steady state
45/276	955	58.15	0.95	0.65	0.80	0.36
45/275	960	53.50	0.89	0.63	0.77	0.34
45/286	1155	46.52	0.40	0.34	0.37	0.08
45/284	1174	58.15	0.30	0.34	0.35	0.07

$$\dot{m}(t) = \dot{m}_0 \frac{1+\beta}{1+\beta \exp(\alpha t)} \tag{22}$$

where α and β are fitted constants.

The time (t_h) for the flow to decay to half its initial value ranged from 0.4 to 10.0 s. Celata *et al.* defined a transient time parameter as follows:

$$t_t = \frac{\rho_{LO} L}{\dot{m}_0} \tag{23}$$

where ρ_{LO} is the liquid phase density at the inlet, L the length of the test section and $\dot{m}_0$ the initial value of the mass flux. Celata *et al.* further defined the parameter τ as

$$\tau = t_h / t_t. \tag{24}$$

They found that the ratio of the mass flux at which dryout occurred in the transient ($\dot{m}_{tr}$) to the mass flux at which dryout would have occurred at the imposed heat flux $\dot{q}(\dot{m}_{ss})$, was a function of τ. Celata *et al.* suggested the following empirical equation to represent their data:

$$\frac{\dot{m}_{tr}}{\dot{m}_{ss}} = 1 - \exp\left[-0.87 p_r^{-0.57} \tau^{0.54} \left(\frac{\dot{q}}{\dot{q}_{ss}}\right)^{2.8/\tau}\right] \tag{25}$$

where $\dot{q}_{ss}$ is the critical heat flux in a steady-state situation for the initial inlet mass flux and p_r the reduced pressure (ratio of pressure to critical pressure).

A total of 18 transient flow calculations were carried out for the conditions of the Celata *et al.* experiments. They were carried out for two different mass fluxes, two different pressures and for t_h ranging from 1 to 7 s. It was not possible to go to smaller values of t_h since the mechanism of the discretization of the code implied that very short time steps would be needed to handle the transients and this would have demanded an excessive amount of computer time. There is no reason in principle why the discretization method could not be changed to accommodate shorter transients and, indeed, this was carried out in some of the earlier work [20]. The calculated and experimental times to dryout are compared in Fig. 9. Most of the predicted times are within $\pm 20\%$ of the experimental values. Bearing in mind the remaining uncertainties (mentioned above) about initial entrainment, the results are considered very encouraging. It was also interesting to plot the predicted results in terms of the empirical correlation of Celata *et al.* embodied in equation (25) above. The results are plotted in this form in Fig. 10. Here, $\dot{m}_{tr}$, $\dot{m}_{ss}$ and $\dot{q}_{ss}$ are all determined by application of the present modelling methods in the steady-state and transient modes, respectively. For the steady-state values, the predicted heat fluxes were within $\pm 4\%$ of the values actually measured by Celata *et al.* in their steady-state flow tests. Figure 10 shows that the predicted values are also consistent with the empirical correlation though, of course, the prediction methodology can be applied over much wider ranges and to any arbitrary fluid and geometry.

6. TRANSIENT REWETTING

The success of the annular flow modelling methodology in predicting transient dryout raises the obvious question about whether the code could be used to predict transient rewetting. Such rewetting would occur where part of the tube is in the post-dryout region and the inlet mass flow rate is increased to cause the tube to rewet. In fact, it is a simple matter to use exactly the same code and procedures to calculate the progress of the rewetting on the assumption that the rewetting front corresponds to the point at

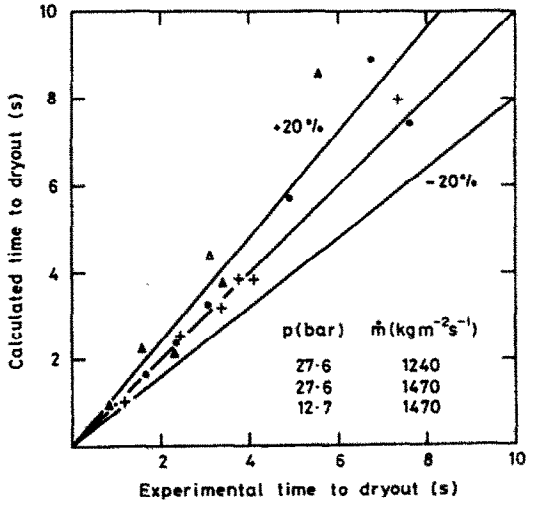

FIG. 9. Comparison of calculated and measured time to dryout.

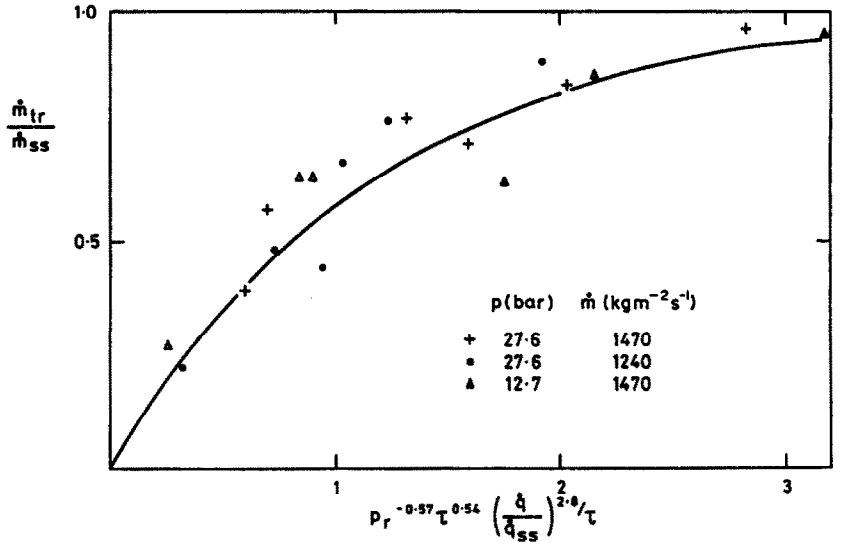

FIG. 10. Comparison of PWJ1A predictions with Celata *et al.*'s transient CHF correlation.

which the film flow rate is zero (consistent with the assumption for steady-state and transient dryout).

Calculations carried out on this basis are illustrated in Fig. 11 for the 70 bar steam–water transient dryout tests of Moxon and Edwards [18]. Consider first a mass flux decreasing with time as illustrated in Fig. 11(a). The transient dryout calculation (described above) predicts a path for the dryout front as shown by curve A in Fig. 11(b). At the imposed value of heat flux ($\dot{q}$) dryout would have occurred in the steady state in a tube of 6.77 m in length. In the Moxon and Edwards experiments, however, the tube length was only 3.66 m. Up to the time of dryout for a tube of the actual length, the predicted dryout length is greater as shown. Dryout actually begins at around 0.8 s when the path of the dryout front meets the end of the actual length of the tube. At the end of the transient, the dryout point is 2.62 m from the tube entrance. If the transient is now precisely reversed, and it is assumed that the rewetting front corresponds (as does the dryout front) to zero film flow rate, then the path of the rewetting is calculated as following curve C (Fig. 11(b)). This implies that the rewetting front reaches the end of the actual tube (3.66 m from the tube entrance) 1.6 s from the start of the mass flow transient. Both the transient dryout and the transient rewet will occur at longer times than would be predicted (curve B) for an unchanging mass flux along the tube. The dryout occurs later because of liquid storage effects and the rewetting occurs later because of the need to 'refill' the liquid film in the tube.

In actual fact, the rewetting process is more complicated than might be suggested by the calculations illustrated in Fig. 11. Once dryout has occurred, the post-dryout region reaches a high temperature (see for instance Figs. 4 and 5) and the rate of rewetting may be governed by the 'sputtering' phenomenon at which the liquid film is essentially blown off the surface as a result of high intensity boiling resulting from axial conduction from the hot, dry zone to the cooler wet zone. This sputtering-type phenomenon has been widely investigated in the context of rewetting transients in nuclear systems. Useful reviews of this work are given by Butterworth and Owen [21] and by Collier [22]. The models for the rewetting phenomenon attempt to describe the balance between the movement of thermal energy towards the rewetting front (it occurs as a result of the motion of a front and also as a result of axial conduction) and the dissipation of this energy in the region immediately upstream of the front by the enhanced heat transfer there. In order to predict the motion of the front, it is necessary to specify the temperature at the front (often referred to as the 'sputtering temperature') and also the heat transfer coefficient immediately behind it. In many models, variation of temperature across the tube wall is ignored (the so-called one-dimensional models), whereas in others it is taken into account (two-dimensional models). For our present purposes, it is sufficient to consider a rather simple model, namely the one-dimensional model of Yamanouchi [23]. Yamanouchi predicted that the rewetting front would proceed at a velocity given by

$$\frac{1}{u_r} = \frac{\rho_w c_{pw}}{2}\left(\frac{\delta}{\alpha(z)\lambda_w}\right)^{1/2}\left(\left[\frac{2(T_w - T_{sp})}{T_{sp} - T_{sat}} + 1\right]^2 - 1\right)^{1/2} \tag{26}$$

where u_r is the rewetting front velocity, ρ_w, c_{pw} and λ_w the density, specific heat capacity and thermal conductivity of the tube wall material, δ the tube wall thickness and $\alpha(z)$ the heat transfer coefficient in the wetted region immediately upstream of the rewetting front. In the Yamanouchi model, $\alpha(z)$ is assumed con-

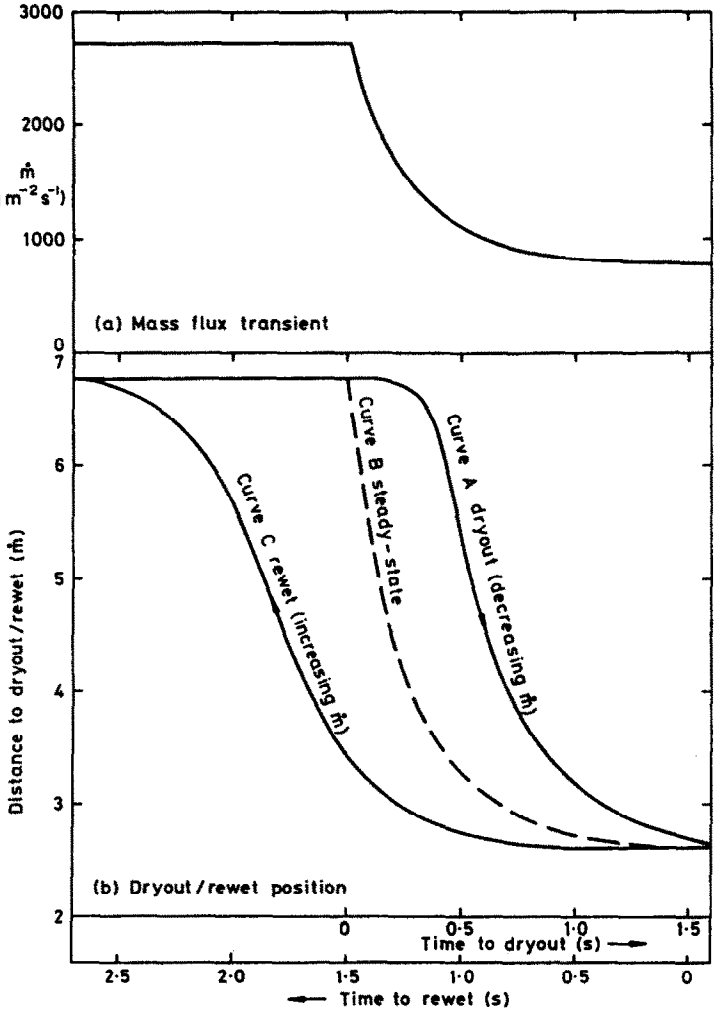

FIG. 11. Movement of dryout/rewet front, assuming zero film flow.

stant, though a whole variety of other models is available in which other forms of variation of $\alpha(z)$ with distance from the rewetting front are assumed. The final variables in equation (26) are the temperatures which are respectively the tube wall temperature downstream of the rewetting front (in the hot, dry region) (T_w), the 'sputtering temperature' (T_{sp}) and the saturation temperature (T_{sat}).

Some illustrative calculations were carried out on rewetting during mass flow transients making the following assumptions.

(1) The fluid conditions and tube diameter were those of the Moxon and Edwards experiment [18], namely water flow at 70 bar in a tube of 10.8 mm i.d. The tube wall thickness was assumed to be 1.63 mm and the material of the wall was assumed to be stainless steel.

(2) The value of α was calculated from the following equation due to Yu *et al.* [24]:

$$\sqrt{\alpha}(T_{sp}-T_{sat}) = 4.24\times 10^4(\dot{m}/\rho_L)^{0.15} \qquad (27)$$

where $\dot{m}$ and ρ_L are the total mass flux and the liquid density calculated at the rewetting front. The remaining required variables are T, the downstream temperature, and T_{sp}, the sputtering temperature.

T_w was estimated from the expected jump in temperature which occurs at the dryout point. This is calculated using the same correlations as those employed in the post-dryout calculations (see Section 3). The temperature immediately after the dryout front can be calculated explicitly since, at this point, the vapour temperature is equal to the saturation temperature and, consistent with the post-dryout heat transfer models, the heat transfer is governed by heat transfer to the saturated steam. Further downstream, the wall temperature becomes higher than that which would be expected for heat transfer to saturated steam since the vapour superheats, despite the presence of the droplets. However, if we are concerned with the rewetting phenomenon, then it could be argued that only the temperatures immediately downstream of the

rewetting front are needed and these are governed by the superheated steam heat transfer. Certainly, the predictions of the post-dryout heat transfer models would indicate that this assumption is not too far out. Thus, T_w is calculable if the local quality at the dryout front is known, as it is in the transient calculation. There is some difficulty about the development of the thermal boundary layer, but for the purpose of simplicity, it is assumed that the fully developed heat transfer equation will apply. The post-dryout models use the Heineman [14] equation for this. The estimation of T_{sp} presents more difficulty. Typically, values of T_{sp} range from 20 to 160 K in excess of the saturation temperature at the system pressure. Yu *et al.* [24] quote quite a wide range of values from various experiments and, in the present illustrative calculations, values of $(T_{sp}-T_{sat})$ of 80 and 160 K were used. The former value is consistent with the measurements of Bennett *et al.* [26] whereas the latter value is consistent with the measurements of Hein and Kohler [27].

As the rewetting front proceeds up the channel, values of α and T_w are calculated instantaneously and the rewetting front velocity u_r estimated. At each point, this velocity is compared with u_0, the rate at which a front would propagate such that the flow rate at the front was zero. This is the velocity calculated from the rewetting by simply reversing the transient dryout calculation, as illustrated in Fig. 11(b). When $u_0 < u_r$, then the rewetting is considered to be governed by the motion of the zero film flow rate front. If $u_r < u_0$, then the rewetting rate would be governed by the axial conduction and the sputtering phenomenon.

Calculations were carried out first for the reversed Moxon and Edwards transient and the results from these calculations are indicated in Fig. 12. Up to approximately 0.4 s, $u_0 < u_r$ and the zero film flow rate limit is dominant (zone AB). After this time the value of u_r becomes less than u_0 and the sputtering phenomenon is dominant. The rewetting process continues to be dominated by this phenomenon for the region BC, and, as can be seen, the sputtering limitation continues for times (for this specific case) which are two orders of magnitude greater than the time required for rewetting on the assumption of a simple

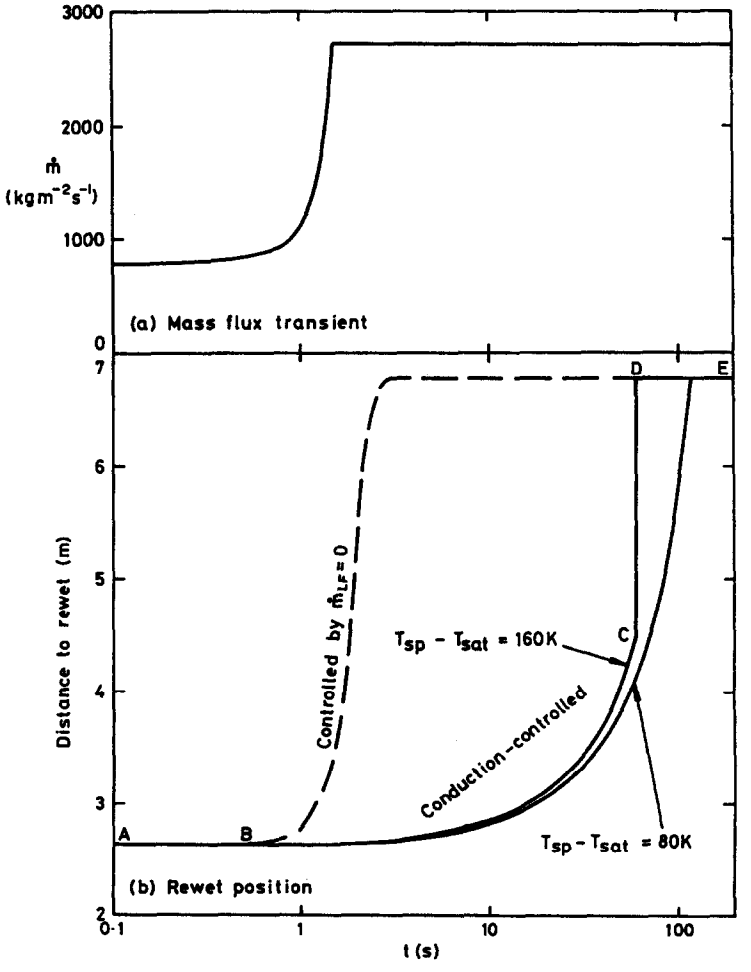

FIG. 12. Movement of rewet front during fast transient.

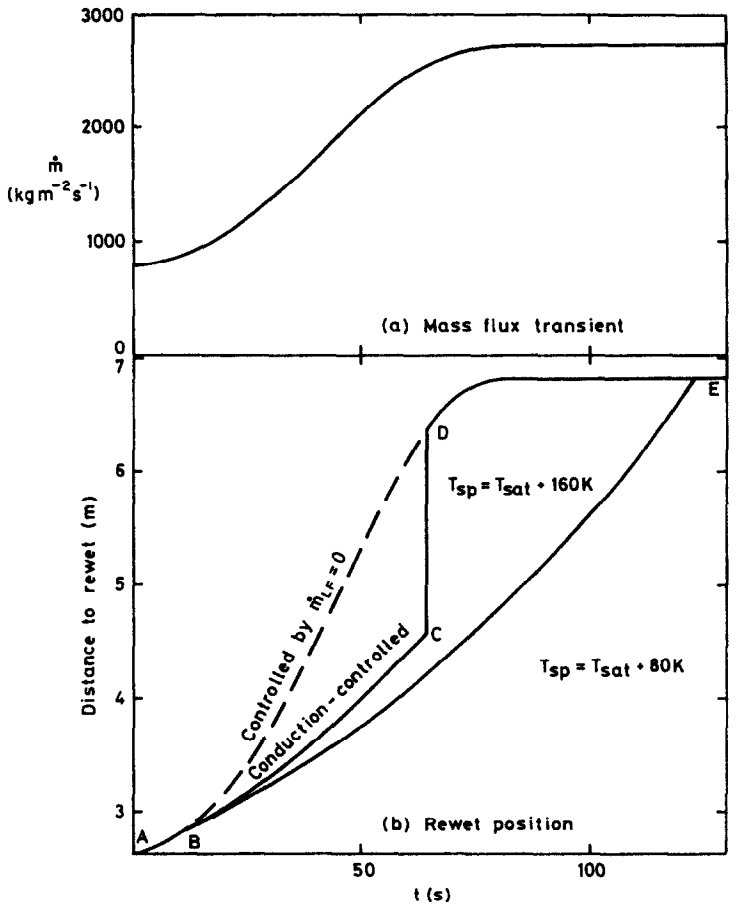

FIG. 13. Movement of rewet front during slow transient.

reversal of the dryout transient. As the rewetting front proceeds up the tube along BC, the quality at the rewetting front is increasing and the value T_w is decreasing. Ultimately, a situation is reached where $T_w < T_{sp}$. At this point, the sputtering effect will be small and (as the experiments of Bennett *et al.* [26] showed), the rewetting front proceeds rapidly along the tube. The rate at which this happens is more difficult to predict; in the present calculations, we have assumed that the remaining part of the tube will rewet at a rate corresponding with the mean film velocity. This was calculated from the local film flow and film thickness values calculated at the rewetting front from the methods described in Section 4. This rapid rewetting (CD on Fig. 12) terminates when the steady-state dryout position is reached at D. Note that this distance is 6.77 m and would, of course, be outside the physical length of tube (3.66 m) used in the original Moxon and Edwards experiments. However, the phenomenon would be expected to follow the pattern shown in Fig. 12 had the tube been sufficiently long.

It is immediately apparent that the behaviour in rewetting will depend on the shape of the mass flux transient. Figure 13 shows some calculations for an alternative, much slower transient and for $T_{sp} - T_{sat} = 160$ and 80 K, respectively. For the higher value of the sputtering temperature, we now see four regions of the curve as follows.

(a) For region AB, $u_0 < u_r$ and the motion of the front proceeds in a manner given by the reverse of the dryout transient.

(b) For region BC, the motion of the front is governed by sputtering and is much slower than the reversed dryout transient.

(c) At point C, the temperature downstream of the front becomes less than the sputtering temperature and the film proceeds rapidly over the surface until point B is reached.

(d) At point D, the film flow rate at the dryout front is again equal to zero and its motion is now governed by the rate at which the film can reach the given distance with zero flow rate at dryout. Eventually, the steady-state dryout position is reached. Also shown in Fig. 13 are the data calculated for $T_{sp} - T_{sat} = 80$ K. In this case, the rewetting continues to be governed by the sputtering phenomenon up to and including the point at which steady-state dryout is reached.

It should be possible to treat any transient in the manner described here to identify the instantaneous governing phenomena and to calculate the rewetting rate. Unfortunately, there is a dearth of data on rewetting during flow transients. However, the qualitative picture shown here is consistent with the observations of Keeys *et al.* [28] for heat flux transients. Moreover, it should be possible to extend the present treatment to deal with the cases of heat flux and pressure transients for which more data are available. In the case of the heat flux transient, it would almost certainly be necessary to take account of the transient response of the wall material.

7. CONCLUSION

Using the new correlations for deposition and entrainment developed in ref. [9] the following new calculations have been carried out on annular flow and related heat transfer.

(1) The new models were applied to the calculation of entrained flow rate in equilibrium and diabatic flows and gave improved predictions of experimental data, compared to previous models of annular flow. A consequence of this improved prediction capability is that the steady-state dryout conditions can be predicted more accurately.

(2) Application of the new models in the context of post-dryout heat transfer also gave improved predictions, though the post-dryout temperatures were sensitive to the precise position of the dryout point which in turn was sensitive, at high mass fluxes, to the assumption about initial entrainment in annular flow.

(3) Predictions for steady-state saturated condensation showed that the entrained flow rate (and hence the film flow rate) could be very different in condensation than for identical quality conditions in equilibrium flows and in evaporation. This was shown to have important consequences on the pressure gradients in these flows.

(4) Calculations on transient dryout indicated that the new models gave closer predictions of dryout in the Moxon and Edwards [18] high pressure steam–water dryout tests. The calculations were also extended to the recent work of Celata *et al.* [19] and shown to predict the transient dryout behaviour for these refrigerant 12 experiments rather accurately.

(5) The new models were employed to carry out some analytical studies of rewetting processes during flow transients. It was shown that the rewetting would probably be governed by either the motion of the zero film flow rate front (the reverse of transient dryout) or by the sputtering process. The governing process would depend on the nature and the stage of a particular transient and would vary with time and distance along the channel.

REFERENCES

1. G. F. Hewitt, H. A. Kearsey, P. M. C. Lacey and D. J. Pulling, Burnout and nucleation in climbing film flow, Harwell Report AERE-R4374 (1963).
2. G. F. Hewitt, H. A. Kearsey, P. M. C. Lacey and D. J. Pulling, Burnout and film flow in the evaporation of water in tubes, *Proc. Inst. Mech. Engrs* **180**, Part 3C, Paper 2 (1965).
3. A. W. Bennett, G. F. Hewitt, H. A. Kearsey, R. K. F. Keeys and D. J. Pulling, Studies of burnout in boiling heat transfer, *Trans. Instn Chem. Engrs* **45**, T319–T333 (1967).
4. A. W. Bennett, G. F. Hewitt, H. A. Kersey and R. K. F. Keeys, Heat transfer to steam–water mixtures flowing in uniformly heated tubes in which the critical heat flux has been exceeded, UKAEA Report No. AERE-R5373 (1967).
5. P. B. Whalley, P. Hutchinson and G. F. Hewitt, The calculation of critical heat flux in forced convective boiling, *Proc. 5th Int. Heat Transfer Conf.*, Versailles, Vol. 4, pp. 290–294 (1974).
6. P. B. Whalley, B. J. Azzopardi, G. F. Hewitt and R. G. Owen, A physical model for two-phase flows with thermodynamic and hydrodynamic non-equilibrium, Paper CS29, 7th Heat Transfer Conf., Munich (1982).
7. P. B. Whalley and G. F. Hewitt, The correlation of liquid entrainment fraction and entrainment rate in annular two-phase flow, Report AERE-R9187, UKAEA Harwell (1978).
8. P. S. James and P. B. Whalley, The calculation of dryout during flow and pressure transients, 2nd CSNI Specialist Meeting on Transient Two-phase Flow, Paris (1978).
9. A. H. Govan, G. F. Hewitt, D. G. Owen and T. R. Bott, An improved CHF modelling code, 2nd U.K. National Heat Transfer Conf., Glasgow (1988).
10. D. G. Owen and G. F. Hewitt, An improved annular two-phase flow model, 3rd BHRA Int. Conf. on Multiphase Flow, The Hague (1987).
11. G. F. Hewitt and N. S. Hall-Taylor, *Annular Two-phase Flow*, Pergamon Press, New York (1970).
12. G. B. Wallis, *One-dimensional Two-phase Flow*, McGraw-Hill, New York (1969).
13. G. B. Wallis, Flooding velocities for air and water vertical tubes, Report AEEW-R123, UKAEA Winfrith (1961).
14. J. B. Heineman, An experimental investigation of heat transfer to superheated steam in round and rectangular tubes, ANL-6213 (1960).
15. G. F. Hewitt, Pressure drop. In *Handbook of Multiphase Systems* (Edited by G. Hetsroni), Chap. 2.2. Hemisphere, Washington, DC (1982).
16. P. B. Whalley, A. J. Lyons and D. Swinnerton, Transient critical heat flux in flow boiling, 1st U.K. Nat. Heat Transfer Conf., Leeds (1984).
17. C. W. Gear, The automatic integration of stiff ordinary differential equations, *Proc. IFIP Congress* (1968).
18. D. Moxon and P. A. Edwards, Dryout during flow and power transient, UKAEA Report No. AEEW-R553 (1967).
19. G. P. Celata, M. Cumo, F. D'Annibale, G. E. Farello and T. Setaro, Flow transients experiments with Refrigerant-12, *Revue Gen. Thermique* 299 (1986).
20. P. B. Whalley, P. W. James and P. Hutchinson, Calculation of the variation of dryout length under transient conditions in two-phase flow, 5th Symp.—Computers in Chemical Engineering, Czechoslovak Chemical Society, Czechoslovakia (1977).
21. D. Butterworth and R. G. Owen, The quenching of hot surfaces by top and bottom flooding—a review, AERE-R7992 (1975).

22. J. G. Collier, Heat transfer in the post-dryout region and during quenching and flooding. In *Handbook of Multiphase Systems* (Edited by G. Hetsroni), Chap. 6.5. Hemisphere, Washington, DC (1982).
23. A. Yamanouchi, Effect of core spray cooling in transient state after loss of coolant accident, *J. Nucl. Sci. Technol.* **5**, 547–558 (1968).
24. S. K. W. Yu, P. R. Farmer and M. W. E. Coney, Methods and correlations for the predictions of quenching rates on hot surfaces, *Int. J. Multiphase Flow* 3(5), 415–444 (1977).
25. A. W. Bennett, G. F. Hewitt, H. A. Kearsey, R. K. F. Keeys and D. J. Pulling, Studies of burnout in boiling heat transfer to water in round tubes with non-uniform heating, AERE-R5076 (1966).
26. A. W. Bennett, G. F. Hewitt, H. A. Kearsey and R. K. F. Keeys, The wetting of hot surfaces by water in a steam environment at high pressure, AERE-R5146 (1966).
27. D. Hein and W. Kohler, Post-CHF heat transfer and rewetting in heated tubes, WRS Mtg, Gaithersburg, Florida (1984).
28. R. F. K. Keeys, J. C. Ralph and D. N. Roberts, Post-burnout heat transfer in high pressure steam–water mixtures in a tube with cosine heat flux distribution, AERE-R6411 (1971).

MODELISATION PHENOMENOLOGIQUE DES ECOULEMENTS HORS D'EQUILIBRE AVEC CHANGEMENT DE PHASE

Résumé—On décrit des calculs de modèles nouveaux pour la déposition et l'entraînement dans un écoulement annulaire avec une variété de conditions d'écoulements annulaires et reliés. Ceci inclut l'écoulement adiabatique permanent, l'écoulement avec évaporation, l'écoulement avec assèchement et dans les régions après assèchement, enfin l'écoulement avec condensation et les écoulements variables. Les cas transitoires incluent les excursions avec un écoulement décroissant (séchage variable) et excursions avec un écoulement croissant (remouillage variable). Lorsque c'est possible les résultats sont comparés aux données expérimentales et on constate que les nouveaux modèles donnent des prévisions améliorées dans chaque cas. Bien que les comparaisons ne soient pas possibles dans le cas des transitoires conduisant au remouillage, quelques aspects nouveaux de ce mécanisme se dégagent de ces calculs. On trouve que le remouillage peut être gouverné soit par la progression d'un front pour lequel le débit de film est nul (l'inverse d'une situation d'assèchement variable), soit par un front dont la vitesse est limitée par le phénomène d'éclaboussure.

PHÄNOMENOLOGISCHE MODELLIERUNG VON NICHTGLEICHGEWICHTS-STRÖMUNGEN MIT PHASENUMWANDLUNG

Zusammenfassung—Es werden Berechnungen beschrieben, in denen neue Modelle für die Deposition und das Entrainment auf eine Vielzahl von Zuständen bei Ringströmung und verwandten Strömungen angewendet werden. Diese beinhalten stationäre adiabate Strömungen, Strömungen mit Verdampfung, Strömungen mit Dryout- und Postdryout-Gebieten, Strömungen mit Kondensation und transiente Strömungen. Bei den transienten Fällen werden die Strömungsabnahme (transientes Austrocknen) und die Strömungszunahme (transientes Widerbenetzen) betrachtet. Wo immer möglich, werden die Berechnungen mit experimentellen Daten verglichen. Obwohl es nicht möglich ist, im Fall der transienten Strömungen Vergleiche zu Experimenten zu ziehen, die zur Widerbenetzung führen, werden einige neue Aspekte zu diesem Vorgang von den Berechnungen abgeleitet. Man stellt insbesondere fest, daß das Wiederbenetzungsverhalten entweder durch das Fortschreiten einer Front mit dem Filmmassenstrom gleich Null bestimmt wird (die Umkehrung des transienten Austrocknens) oder durch eine Front, deren Geschwindigkeit durch das Phänomen des Sprühens begrenzt ist.

ФЕНОМЕНОЛГИЧЕСКОЕ МОДЕЛИРОВАНИЕ НЕРАВНОВЕСНЫХ ТЕЧЕНИЙ С ФАЗОВЫМИ ПЕРЕХОДАМИ

Аннотация—Проведены расчеты, в которых новые модели образования пленок и уноса капель при кольцевом течении используются применительно к целому ряду процессов, наблюдаемых при таком и подобных течениях: стационарном адиабатическом, с испарением, с образованием критических и закритических областей, с конденсацией и переходными режимами. В последних имеют место как рост скорости течения (переходное критическое состояние), так и ее уменьшение (переходное повторное смачивание). Проведено сравнение, где это возможно, результатов расчетов с экспериментальными данными, которое показало, что новые модели дают более точные значения для каждого случая. Хотя сравнение с экспериментальными данными для переходных состояний, приводящих к повторному смачиванию, невозможно, расчеты позволили выявить ряд новых аспектов процесса. В частности, найдено, что интенсивность образования пленки может определяться процессами на фронте, когда либо расход пленки равен нулю (ситуация, обратная переходному критическому состоянию), либо скорость фронта ограничена явлением разбрызгивания.